

Article

Enhancing the Performance and Durability of Commercial Vehicle Cargo Box Frames through Modal Analysis

Nitisak Numanoy ¹, Kontorn Chamniprasart ² and Jiraphon Srisertpol ^{2,*}

¹ Department of Mechanical Engineering, Faculty of Engineering and Technology, Rajamangala University of Technology Isan, Nakhon Ratchasima 30000, Thailand; nitisak.nu@rmuti.ac.th

² School of Mechanical Engineering, Institute of Engineering, Suranaree University of Technology, Nakhon Ratchasima 30000, Thailand; kontorn@sut.ac.th

* Correspondence: jiraphon@sut.ac.th

Abstract: The cargo box frame (CBF) is the main structure of a commercial vehicle designed to handle loads and components during travel. The chassis is subject to vibrations caused by rough roads and the components mounted on it. This study proposes a procedure for analyzing and validating CBF structures using a combination of non-destructive modal analysis and finite element analysis to investigate the vibration characteristics of the four-wheel CBF, including its natural frequency and mode shapes. The CBF's response to various load conditions, including stress distribution and displacement, was analyzed. The results show that the actuation frequency can affect a truck's chassis due to the CBF's natural frequency falling within the excitation range. The resulting mode shape can improve CBF strength, reduce weight, identify defective welds, and determine optimal mounting locations based on the center of gravity (CG) for components such as side-swing doors and cold room panels.

Keywords: commercial vehicle; cargo box frame; non-destructive modal analysis; vibration characteristics; finite element analysis; securing basic performance; safety requirements



Citation: Numanoy, N.; Chamniprasart, K.; Srisertpol, J. Enhancing the Performance and Durability of Commercial Vehicle Cargo Box Frames through Modal Analysis. *Appl. Sci.* **2023**, *13*, 9303. <https://doi.org/10.3390/app13169303>

Academic Editor: Marco Troncosi

Received: 17 April 2023

Revised: 31 July 2023

Accepted: 10 August 2023

Published: 16 August 2023



Copyright: © 2023 by the authors. Licensee MDPI, Basel, Switzerland. This article is an open access article distributed under the terms and conditions of the Creative Commons Attribution (CC BY) license (<https://creativecommons.org/licenses/by/4.0/>).

1. Introduction

The consideration of actual welding processes can have an impact on the complexities and uncertainties involved in the Finite Element Analysis (FEA) of structures. FEA utilizes welding models to approximate the effects of the welding process. However, these models may not accurately replicate the actual welding process, resulting in discrepancies between FEA results and the actual welded structure. Determining accurate welding parameters for FEA analysis can be challenging, especially in the case of complex welded structures. Welded joints may possess different material properties compared to the base structure. FEA typically assumes constant material properties, which may not accurately represent the variations in material properties caused by welding. The welding of multiple components can influence the stiffness and natural frequency of the structure. To address these limitations, it is crucial to refine the welding models employed in FEA and validate them using testing data. Additionally, conducting iterative testing and adjusting parameters based on experimental data can enhance the accuracy of FEA analysis for structures with multiple welded components.

Numerous vehicle owners opt to modify or alter their registered vehicles. However, in the absence of proper control or supervision to ensure compliance with automotive engineering principles and appropriate safety standards, this can pose a threat to both the vehicle owner and other road users. Additionally, such modifications may create opportunities for illegal activities. Therefore, it is essential to establish specific criteria to permit vehicle modifications or alterations to ensure compliance with international standards and guarantee safety. The Land Transport Act of B.E. 2522 (1979) is among the regulations that Thailand has utilized to define the following terms [1]:

- Land transportation refers to the transportation of people, animals, or goods by road using vehicles.
- Regular transportation refers to transportation for hire on routes designated by the Transport Committee.
- Small-scale transportation refers to transportation of people or goods, or a combination of both, for hire on routes designated by the transport committee, using vehicles with a combined weight of no more than 4000 kg.
- Personal transportation refers to transportation of goods for one's own business using vehicles that weigh more than 2200 kg.
- A pickup truck is defined as a vehicle that has a solid, box-shaped section for carrying cargo with a permanent roof. The cargo area and the driver's compartment may be integrated together or separated, and there may be doors for loading on the side or rear. It is classified as the second type of vehicle used for transporting animals or goods from among the nine types.

The regulations cited in this passage include the Vehicle Act (No. 3) of B.E. 2525 (1982), as well as Sections 12 and 14 of the Vehicle Act, B.E. 2522 (1979), and Section 4 of the Land Transport Department Regulation on Criteria for Requesting and Granting Permits for Modified Vehicles under the Vehicle Act, B.E. 2562 (2019). According to these regulations, "vehicle" refers to personal cars and motorcycles, "chassis" refers to the original manufacturer's framework that supports the weight and cargo of the vehicle, and "body" pertains to the driver's seat and passenger compartment, but excludes the cargo area. Vehicles that have undergone reinforcement, modification, or installation of additional parts are considered to be unlawfully altered, specifically pickup trucks. Nonetheless, this can be rectified by informing the Department of Land Transport where the vehicle is registered about the modification. Failing to report such modifications would be considered a breach of the Land Transport Act of B.E. 2522. As of September 30, 2022, the total number of trucks in Thailand was 1,217,179. Compared to September 30, 2021, there was an increase of 397,122 trucks that are not fixed-route, representing 32.63% (an increase of 5.57%). The type of truck that saw the highest increase was pickup trucks at 6.96%, followed by semi-trailers with a total of 98,208 vehicles (representing 24.73% of the total) and pickup trucks with a total of 94,085 vehicles (representing 23.69% of the total) [2].

The cargo box trucks (CBTs) of the single cab type are designed for chassis applications in Thailand, with a focus on providing a dependable service for an extended period. These trucks are adaptable to meet various chassis requirements due to their diverse cargo box sizes and configurations. Moreover, the CBFs possess the flexibility and capacity to produce highly customized truck bodies that can satisfy the most challenging applications. The Body Builder's Guide for HILUX 2020 by Toyota Motor Corporation [3] states that all body-builders must prove that their body modifications do not affect the fundamental functions of the base vehicle. Additionally, they must conduct comprehensive research to ensure that any changes made to the standard parts do not create functional or safety issues from both technical and safety perspectives. There are discussions on safety factors in the structural integrity assessment of components with defects [4], focusing on the structural analysis of ladder chassis for higher strength [5], and examining the calculation of safety factors according to the Eurocodes [6]. Gulvanessian, Calgaro, and Holicky provide a designer's guide to EN 1990, EUROCODE, which serves as the basis for structural design [7].

The body modifications or alterations should not obstruct the forward area of view, damage the chassis frame, or cause an imbalance in weight between the right and left wheels. To avoid the local concentration of load on the chassis frame, the body-building job must be conducted in a way that distributes the load evenly over the frames, ensuring that all the wheels are positioned on the same plane without distorting the frame. Additionally, the materials and parts used in the body-building or alteration work should be designed and fabricated to facilitate the inspection and maintenance of the chassis parts once they are mounted on the vehicles. There are specific limitations on the length, width, height,

and weight of the parts installed according to each specific base vehicle, and it is necessary to comply with any additional restrictions that may be enforced in each country.

The research articles cover various aspects of modal analysis and its applications in different fields. Modal analysis is explored in various contexts within the collection of articles. It encompasses powertrain modal analysis for vehicle drivability studies [8] and modal analysis applied to a conceptual microsatellite design featuring perforated structural components for mass reduction [9]. The utilization of the digital image correlation technique is presented for modal analysis [10], along with an exploration of vibration fatigue analysis of carbon steel coil springs under different road excitations [11]. Furthermore, novel modal testing methods designed for structures rotating in water are assessed [12]. Additionally, the research focuses on the operational modal analysis of an axial compressor rotor and casing system, aiming to identify a digital twin online [13], as well as the modal analysis of lithium-ion batteries for electric vehicles [14]. Strain modal testing using fiber Bragg gratings is investigated specifically for automotive applications [15].

In the automotive industry, modal analysis technology plays a significant role. It is extensively applied in studying the dynamic response analysis of vehicle suspension systems, load reverse engineering [16], and vibration fatigue analysis for designing rapid box wagons [17]. The articles also delve into the vibration characteristics of a full-side open boxcar [18] and the effects of adding an auxiliary chassis to a 6-ton truck [19]. Overall, this research highlights the importance of modal analysis and vibration analysis in various engineering fields. It showcases a wide range of techniques and applications that aid in identifying potential structural weaknesses, and enhancing durability, reliability, and performance. Specifically, the presented article introduces an analytical modeling approach to enhance structural analysis by understanding acoustic emission signals in thin-walled objects [20]. It proposes a novel intelligent method for bearing fault diagnosis that employs EEMD permutation entropy and GG clustering to improve accuracy and efficiency [21]. Furthermore, it introduces a new online operational modal analysis method for vibration control in linear time-varying structures, offering real-time monitoring and adjustment capabilities [22]. Additionally, the article investigates the application of empirical mode decomposition and artificial neural networks for automatic bearing fault diagnosis based on vibration signals, aiming to achieve reliable and efficient fault detection [23].

Understanding the modal behavior of a car chassis is crucial for analyzing its dynamic behavior. The vibrational characteristics of a vehicle depend on its stiffness and mass distribution. Global bending and torsional vibration mode frequencies are often used to evaluate the structural performance of a vehicle. Bending and torsional stiffness are critical for the vibrational behavior of the structure, especially its first natural frequency. Therefore, to enhance the performance and durability of the entire CBF, a combined simulation and test-based method is used for conducting dynamics analysis of the CBF, based on simulation analysis and vibration test results.

This paper is structured as follows: Section 2 presents the research methodology and materials used. Section 3 analyzes the results and provides validation for both simulation and experimental performance analysis. Section 4 interprets the differences found in the requirement expression characteristic analysis. Lastly, Section 5 presents the conclusions derived from the proposed technique.

2. Materials and Methods

2.1. Non-Destructive Modal Analysis

Modal analysis is the process of determining modal parameters of mechanical systems that describe their dynamic behavior. It can be approached theoretically, numerically, or experimentally. Theoretical modal analysis involves solving the eigenvalue problem of the mathematical model of a mechanical system. The equations that describe the linearized motion of a general form in a particular configuration are provided by

$$M\ddot{q}(t) + D\dot{q}(t) + Kq(t) = f(t) \quad (1)$$

where \mathbf{M} , \mathbf{D} and \mathbf{K} are the mass matrix, the damping matrix and the stiffness matrix, respectively. The vector $\mathbf{q}(t)$ contains the degrees of freedom (DOF) of the system.

Equation (1) is a set of differential equations in matrix form for the dynamic response of a structure modelled with a finite number of degrees of freedom. An eigenvalue analysis, commonly known as the most prevalent form of dynamic analysis, is often performed. Apart from determining the frequencies, it is also essential to investigate the mode shapes that occur at the natural frequencies. These mode shapes represent the undamped free vibration response of the structure resulting from an initial disturbance from its static equilibrium position. To obtain this solution, the damping and applied force terms in the general equation are neglected. Subsequently, it is assumed that each node experiences sinusoidal functions ($\mathbf{q} = \mathbf{A} \sin(\omega t)$) with peak amplitudes specific to that node. The number of eigenvalues or natural frequencies in the model is equal to the total number of DOFs. Each eigenvalue or frequency is associated with a corresponding eigenvector or mode shape. Since none of the eigenvectors can be zero vectors ($\mathbf{A} \neq 0$), the equation that needs to be solved is as follows:

$$(\mathbf{K} - \omega^2 \mathbf{M}) = 0 \quad (2)$$

It is important to mention that our typical focus lies on the first few eigenvalues of the model. This is because the finite element model, being an approximation of the structure, tends to yield inaccurate higher eigenvalues and vectors. According to the theoretical solution, the structure exhibits indefinite vibrations in various mode shapes. However, due to the presence of damping in all structures, these vibrations ultimately decay over time.

Modal parameters are determined through measurements, which is an experimental approach. This involves recording the time histories of excitation force and corresponding response of the system. The system's dynamic behavior can be described in the frequency domain using the frequency response function (FRF) or in the time domain using the impulse response function (IRF). These functions are calculated from measurement data using the Inverse Fourier Transform. Impact testing has become the most popular method for experimental modal analysis as FRF measurements can be computed using a FFT analyzer. Impact testing is a fast, convenient, and low-cost way of finding the modes of machines and structures.

The FRF is defined as the ratio of output signal to input signal. There are three primary types of FRFs based on the type of response parameter being analyzed. These response parameters can be displacement, velocity, or acceleration in relation to frequency. A set of all the FRFs is called frequency response function matrix. Furthermore, the Laplace transform ($s = i\omega$) and neglecting initial conditions in the frequency domain of Equation (1) are given by

$$\mathbf{Q}(s) = \mathbf{H}(s)\mathbf{F}(s) \quad (3)$$

where $\mathbf{H}(\omega) = (\mathbf{K} + i\omega\mathbf{C} - \omega^2\mathbf{M})^{-1}$ is called the transfer function matrix. The definition of one element of FRF matrix for receptance is as follows:

$$\mathbf{H}(\omega) = \Phi[(\lambda_r^2 - \omega^2)]^{-1}\Phi^T \Rightarrow H_{jk}(\omega) = \sum_{r=1}^n \left(\frac{\phi_{jr}\phi_{kr}}{\lambda_r^2 - \omega^2} \right) \quad (4)$$

where λ_r is eigenvalue of the r -th mode, ϕ_{jr} is the j -th element of the r -th natural shapes vector, and n is number of modes. The vibration modes are determined from the FRF or IRF by applying special estimation procedures. Each mode is characterized by the natural frequency, damping ratio and mode shape. These characteristics, commonly called modal parameters, contribute to the understanding and utilization of proper orthogonal decomposition in the analysis and modeling of vibrational behavior in mechanical and structural systems [24,25].

2.2. Finite Element Modeling

This methodology involves the FEA of CBF followed by design. The pre-processing stage in the simulation involves CAD modelling, meshing and applying loads and boundary conditions. The solution stage involves element matrix formulations, and the assemblage of global stiffness elements followed by inversions and multiplications. The final stage is post-processing, which involves viewing and editing the results.

The CAD model of the CBF was created in the SolidWorks referring to the frame drawing and body attachment holes of a single cab, as shown in Figure 1. This model is simulated using the ANSYS software, V18.1 version. The overall view orientation is shown in Figure 2. Limitations are set for the length (L), width (W), height (H) and weight of the parts mounted according to the particular base vehicle. Any restrictions which may be imposed in each country should be complied with. The simulation used in this research is the modal analysis for model validation to compare with the EMA, after which this CAD model is used to evaluate the effect of static structural analysis.

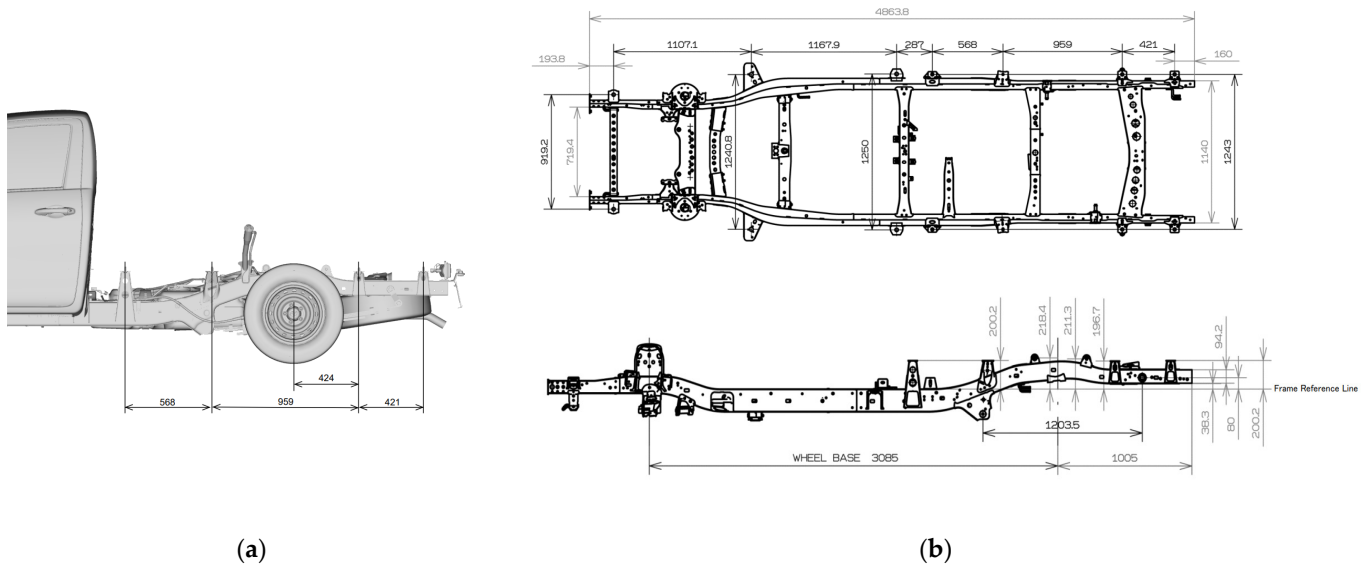


Figure 1. Frame drawing of single cab and chassis dimensions [3]: (a) holes; (b) long wheel base.

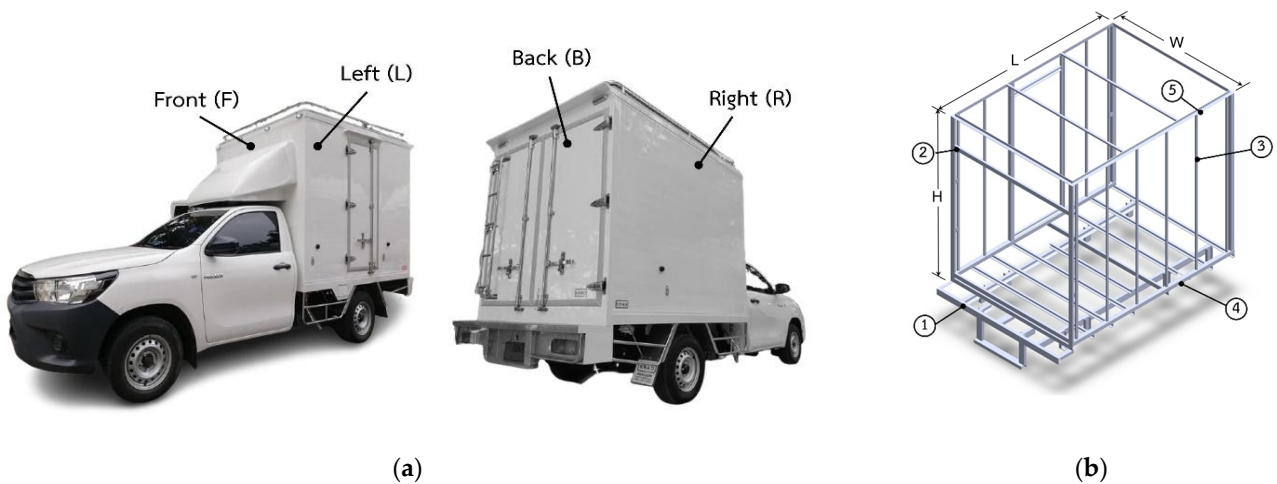


Figure 2. View orientation of CBT and CBF: (a) perspective views of commercial vehicle; (b) CAD modelling.

The physical and mechanical properties are shown in Table 1. The software is used to determine the dynamic characteristics such as natural frequencies and the corresponding

mode shapes of the CBF. The hot rolled structural steel (SS400) material is defined in the property of the static structural and modal modules in ANSYS software. The following in Table 1 shows the Thai Industrial Standard (TIS) of SS400 material mechanical properties, such as the yield point or yield strength (yield stress), tensile strength and elongation. Convergence studies about element size were performed and optimum element sizes were selected as 10 mm. In the finite element model of the CBF, 552,400 elements of hybrid grid type were used. Hybrid grids combine the advantages of structured (quadrilateral) and unstructured (triangular) elements, enabling efficient meshing in areas where structured grids are suitable, as well as handling complex regions with unstructured elements. They are particularly useful for the intricate or highly distorted geometries of the CBF. The initial testing was subjected to a free-free boundary condition, where it was supported by a chain hoist. This condition was then modeled in Ansys Workbench, simulating a free-free condition without any imposed restrictions on the boundary conditions. Specifically, none of the DOFs under the body attachment holes of the CBF were constrained or selected.

Table 1. Mechanical properties of the CBF (thickness < 16 mm).

Type	Size	Classifications	Yield Point	Tensile Strength	Elongation
	inch × inch		MPa	MPa	%
C-channels	① 3 × 1½	TIS 1227	245	400–510	18–23
	② 2 × 1				
Square tube	③ 1 × 1	TIS 1228	245	400–510	18–23
	④ 2 × 2				
Equal angle	⑤ 1½ × 1½	TIS 1227			

Number ① to ⑤ refers to Figure 2b.

2.3. Securing Basic Performance and Safety Requirements

For the purpose of ensuring safe operation, an even distribution of the cargo weight across the entire vehicle is assumed. The ratio provided below should be employed to ascertain the load exerted on the front axle:

$$\text{Ratio} = \frac{F_r}{T} \times 100\% \geq 30\% \quad (5)$$

where F_r is the front axle mass and T is the total vehicle mass. The mass checks are measured the curb mass of the built or altered vehicle. Take a measurement of the front axle mass (F_r) and the rear axle mass (Re) separately. Each value must not be more than their respective tolerances. The relation between the overall vehicle mass and maximum allowable axle weight is as follows:

$$G.V.W \geq F_r + Re \quad (6)$$

and

$$B \leq G.V.W - (C.W. + A) \quad (7)$$

where the A defines the special equipment, accessories and permanent attachment. The B is the total mass of passengers, cargo and baggage.

3. Experimental Investigation and Results

The following are the steps for analyzing and designing the structure:

- Modal Test and Model Validation: these are the steps for modeling and analyzing the CBF structure:
 - a. Measure various dimensions of the commercial vehicle and create a three-dimensional structure of CBF using SolidWorks software.

- b. Test the main structure characteristics using a modal testing technique by classifying the behavior of different frequencies.
 - c. Simulate vibration behavior at different frequencies using a finite element method in Ansys software.
 - d. Compare the accuracy of test results with the model to use in statistical analysis.
 - e. Simulate damage analysis with Ansys software under various conditions.
- Refinement and Enhancement: Adjust the local center of gravity position of the supporting structure for the refrigerated cabinet. Analyze the results of the model structure to propose solutions:
 - a. Adjust the local center of gravity position of the supporting structure for the refrigerated cabinet.
 - b. Change the supporting metal structure for the refrigerated cabinet.
 - The secure running safeties: compare the results before and after improvements.

3.1. Modal Test and Model Validation

This section describes the experiments required to perform a modal analysis on the CBF. Non-parametric system identification is applied to the input and output spectra to obtain a set of FRFs. The first step in the procedure is to measure the impulse response of a system, by means of an impact test. This is performed using an impact hammer and tri-axial acceleration sensors. A data acquisition module is utilized to measure the input and output signals between each excitation point and measured output. Analog signals are converted into discrete time signals by the module, which are then communicated to the computer at fixed time intervals specified by the sampling frequency. These input and output signals are transformed to the frequency domain by means of the Discrete Fourier Transform. These transformed signals are used to calculate the FRFs.

The following equipment is required to perform an impact test:

1. The free boundary condition is subject to limitations imposed by the natural frequencies of the rigid body modes. To investigate the dynamic behavior of a CBF, it is suspended from a chain hoist, creating one or more rigid body modes based on the stiffness of the supporting materials and the total mass of the structure. If the natural frequencies of these rigid body modes are significantly different from the first natural frequency of the structure, the measured FRF data should not be affected by this boundary condition.
2. The 3D motion at each test point is desired in the resulting mode shapes. A roving tri-axial accelerometer is used and the CBF is impacted at a fixed DOF with the hammer. The locations in the structural testing refer to the 3D wireframe model (208 points) of CBF, shown in Figure 3. The tri-axial accelerometer must be simultaneously sampled together with the force data; a four-channel FFT analyzer is required instead of a two-channel analyzer.
3. The data-acquisition device DT9837B is used with the IEPE signal conditioning unit. This device is a high-accuracy dynamic signal acquisition module that is ideal for vibration measurements. It contains four synchronized 24-bit sensor inputs that provide a data stream that is matched in time, which can be used for signal analysis. During the tests, only one SIMO transfer is measured, using one impulse force hammer (type 9722A500) and one tri-axial accelerometer (type 8763B100) from KISTLER.

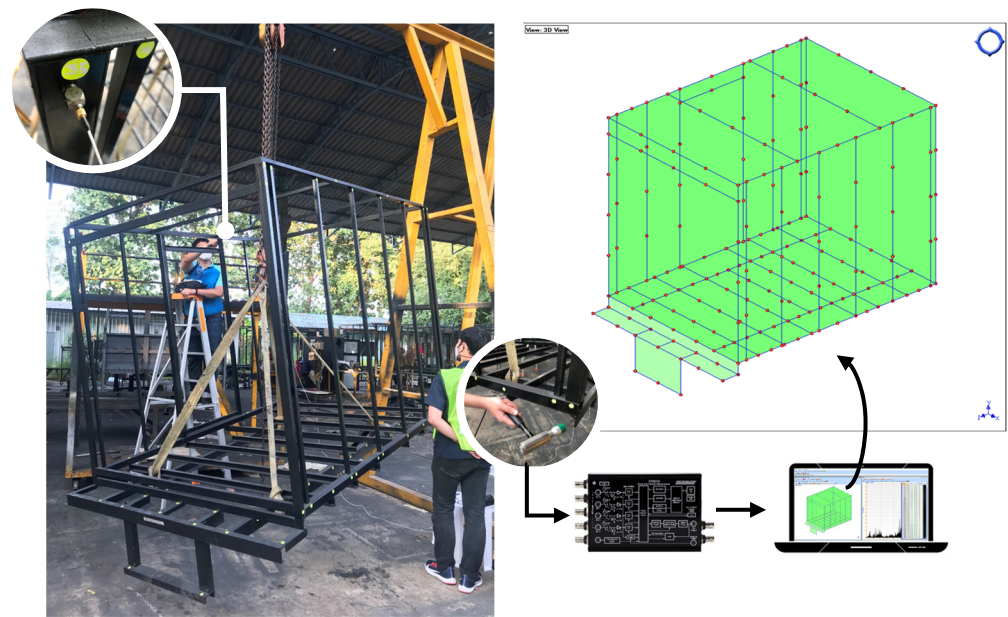
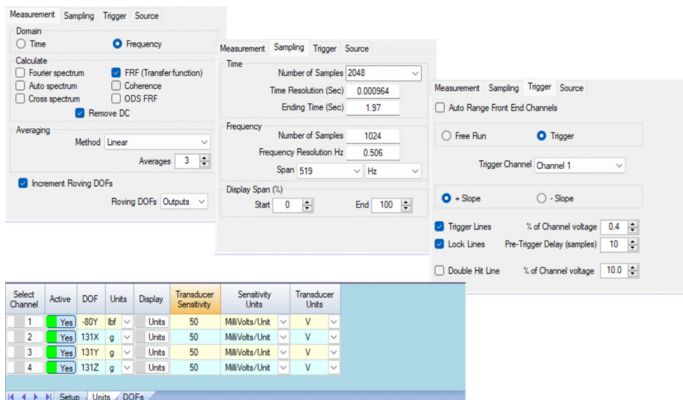


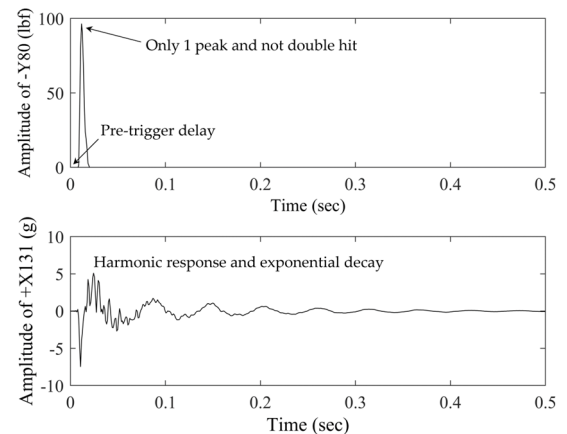
Figure 3. Structural testing refer of the 3D wireframe model of CBF.

4. Sampling frequency, also known as sampling rate, refers to the number of samples taken per unit of time during the process of digitizing an analog signal. It represents the rate at which the continuous analog signal is discretized into discrete samples. The choice of an appropriate sampling frequency depends on the characteristics of the signal being sampled and the specific requirements of the application. Higher sampling frequencies capture more detail and allow for the accurate representation of high-frequency components, but they also require more storage and computational resources. Let us define the sampling frequency for our testing based on the number of samples and frequency span in the FRF setup as 4096 lines and 1024 Hz. According to Nyquist's theorem, we can only accurately measure frequencies up to half of the sampling rate. Therefore, the sampling frequency should be set at least twice the maximum frequency component present in the signal. So, our spectral line resolution is calculated as half of the sample rate divided by the number of lines, resulting in 0.5 Hz. The window calculation time is 2 s. Each experiment is repeated at least three times, and the best three measurements are used to determine the averaged FRF for the corresponding SIMO transfer.

Setting up the signal processing: During the measurement, choose the frequency domain and select the FRF (transfer function) for calculation. Use the linear method for averaging and set the number of repetitions to three times. Regarding sampling, set the number of samples to 2048 in the time domain. In the frequency domain, set the maximum frequency to 1280 Hz. Other values will be calculated based on these two parameters. For the trigger configuration, select the trigger type and use Force Channel 1 (connected to the acquisition device, DT9837B) as the reference port. Choose the +slope of the trigger and set the trigger lines and lock lines to observe and adjust the time signal from the hammer impact, as shown in Figure 4a. In this test, use 0.4% of the channel voltage and set a pre-trigger delay of 10 samples. In the setup for the channels spreadsheet, activate four channels and select AC Coupling for one of the piezoelectric force hammers and for the other three channels, connect them to accelerometers. Set the force unit as lbf and the acceleration unit as g. Enter the sensitivity constant of 50 mV/unit for all the transducers (using the instrument's datasheet). During impact testing, use the force window for the hammer channel and the Hanning window for the acceleration channel.



(a)



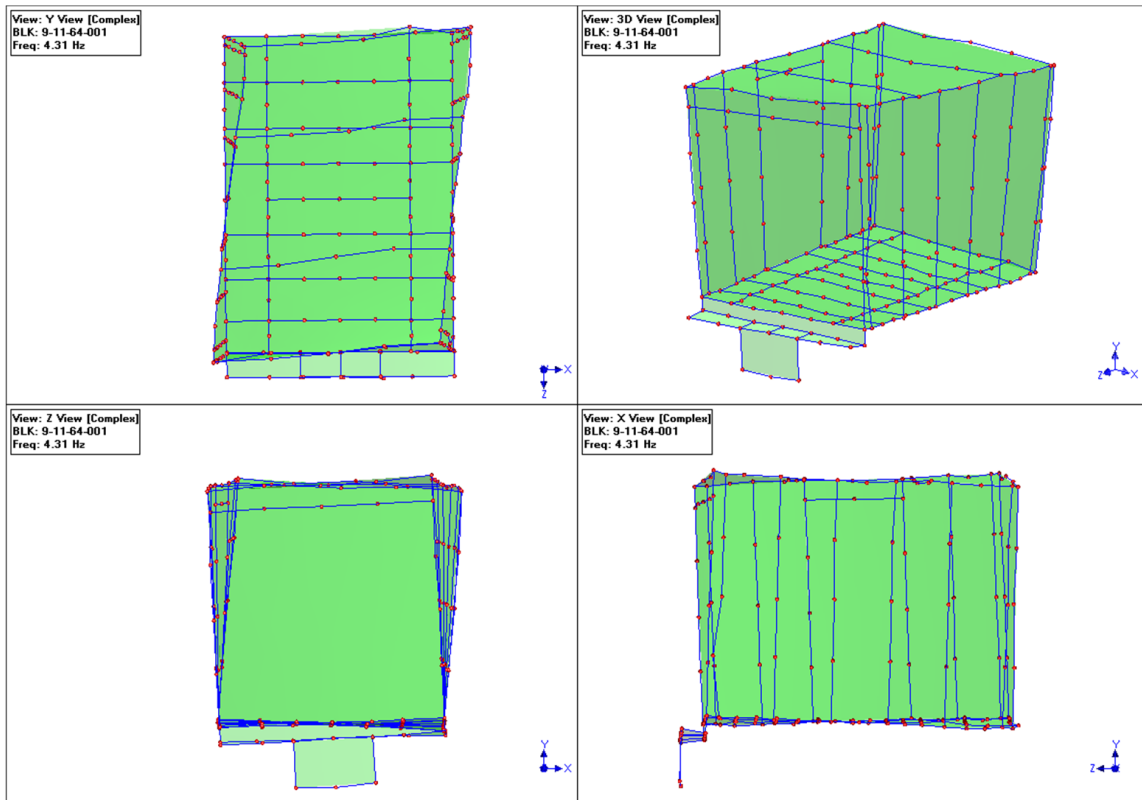
(b)

Figure 4. (a) Setting up the processing using acquisition; (b) force and acceleration signal.

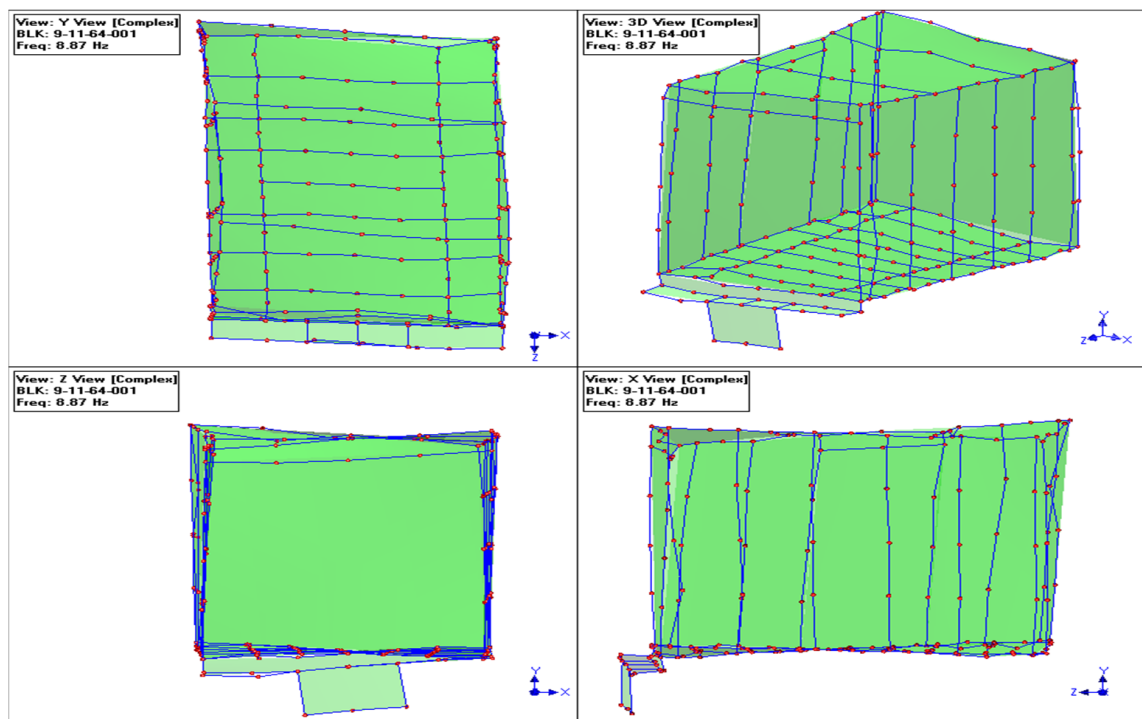
Precautions to be taken during signal acquisition: It is essential to carefully examine the response results each time an impact is applied to ensure that the signal patterns are suitable for subsequent signal processing, as shown in Figure 4b. This is particularly important because 208 data points are collected for the FRF, and all three directions of response are measured using accelerometers, resulting in a total of 624 functions. Furthermore, it is not feasible to collect response data in the time domain. Therefore, it is necessary to observe the response results only during the data acquisition process. For instance, let us consider the measurement at point 80 in the $-Y$ direction (denoted by a negative sign, indicating the opposite direction of the reference installation of the accelerometer) compared to point 131 in the $+X$ direction. The response results in the time domain are depicted in Figure 4b. In this specific test, point 80 in the $-Y$ direction is selected as the impact location using a hammer, and roving accelerometers are employed to measure the response at the designated position, which is point 131 in the $+X$ direction on the structure.

- The responses of the CBF are acquired in the tri-axial accelerometer and hammer data acquisition system and then transferred into MScope software. For parameter estimation of the CBF, the experimental modal analysis (EMA) software [26] is used. The CBF tests are conducted under predetermined environmental conditions. The frequency span of 0–25 Hz is chosen for the model validation.
- The modal identification is performed using a technique of extraction in the peak picking method from the power spectral densities. This technique provides estimations of the natural frequencies and mode shapes. The first six mode shapes obtained from this method are shown in the next part to compare with the simulation, and Figures 5–7 illustrates the demonstration of the motion snapshot of the CBF at 4.31 Hz to 23.8 Hz, respectively. If a CBF is excited near one of its frequencies, the corresponding mode shape will dominate. However, there will still be a small contribution from all other modes present in this response.

The road excitation from the transmission system has typical values varying from 0 to 100 Hz. In practice, diesel engines are known to have an operating speed of about 8 to 33 Hz [19]. In the low-speed idling condition, the excitation frequencies are about 8 to 10 Hz. The main excitation is at low speeds, when the truck is in the first gear during the idling condition of engine. At higher gears or speed, the excitation to the chassis is much less.

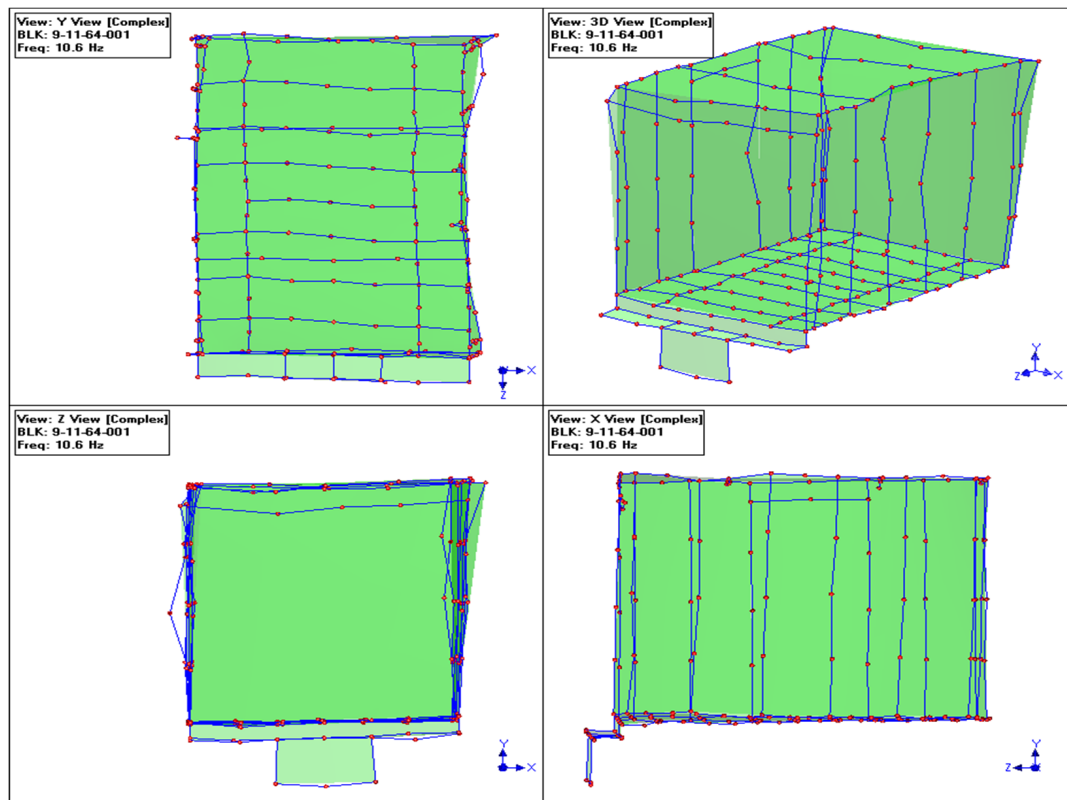


(a)

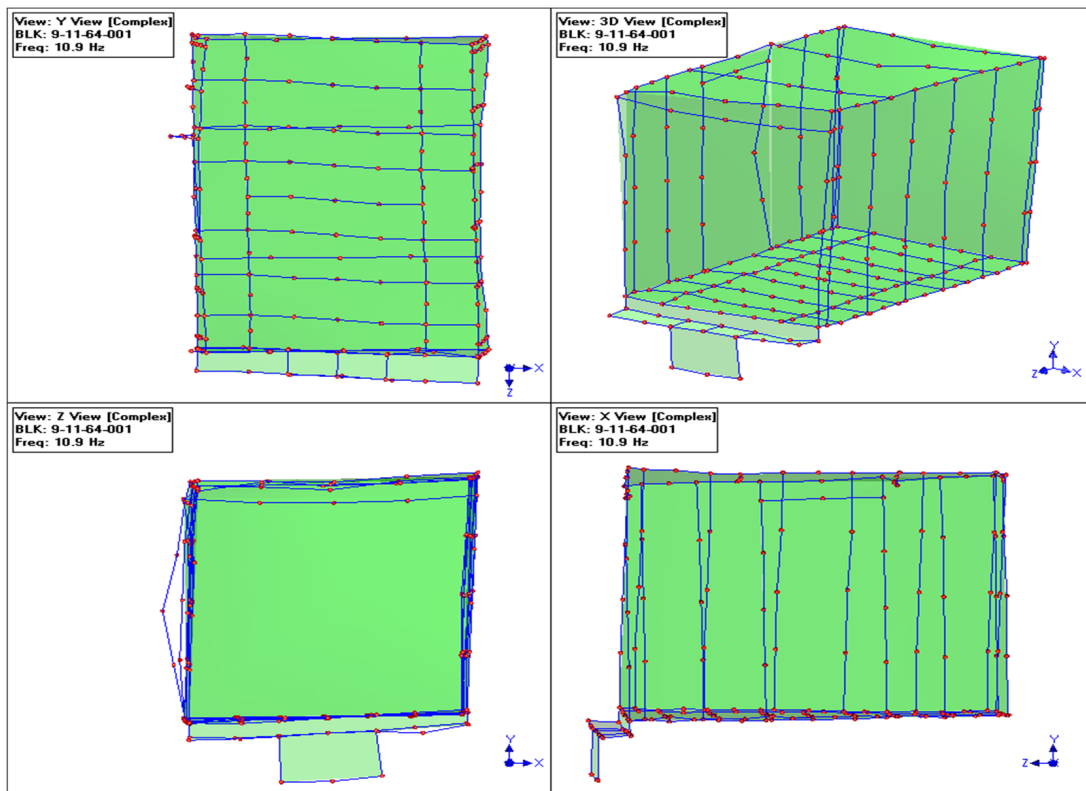


(b)

Figure 5. Motion snapshot from relative maximum deviation behavior of EMA: (a) at 4.31 Hz; (b) at 8.87 Hz.

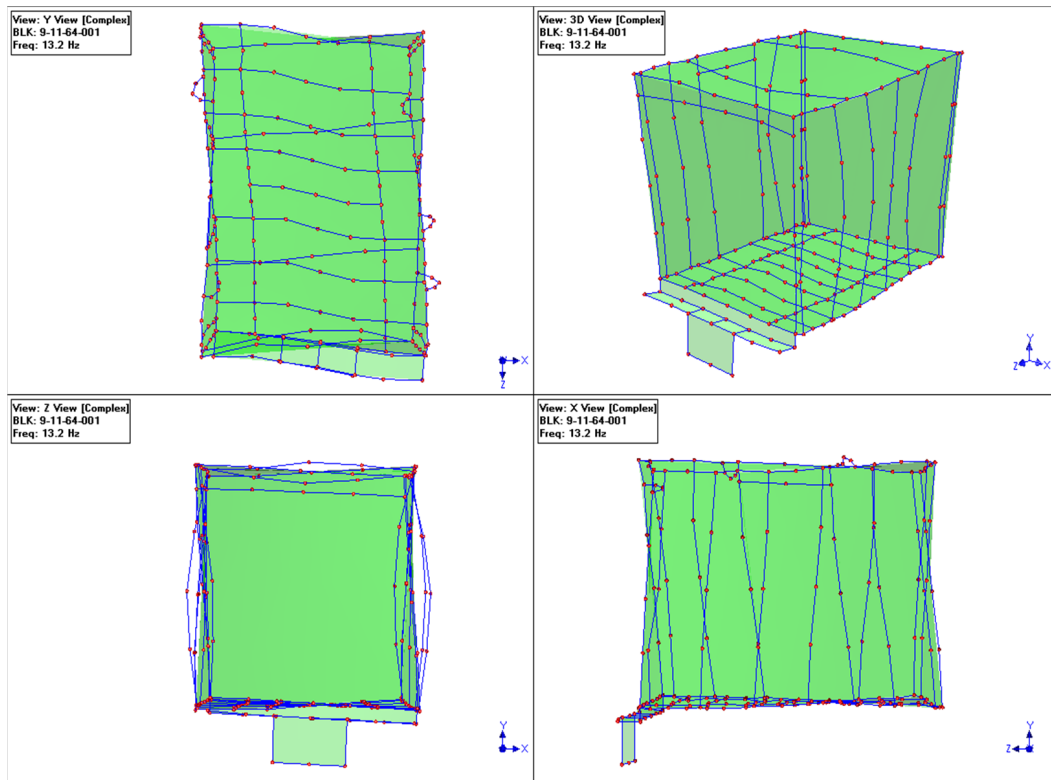


(a)

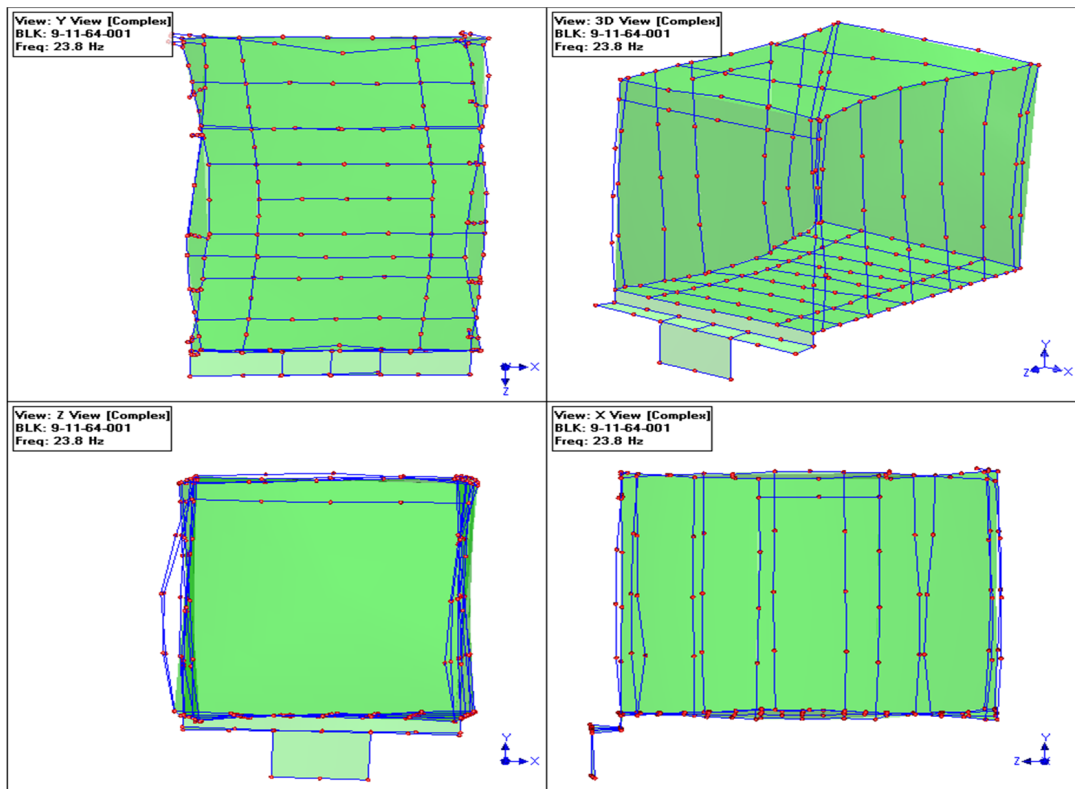


(b)

Figure 6. Motion snapshot from relative maximum deviation behavior of EMA: (a) at 10.6 Hz; (b) at 10.9 Hz.



(a)



(b)

Figure 7. Motion snapshot from relative maximum deviation behavior of EMA: (a) at 13.2 Hz; (b) at 23.8 Hz.

The natural frequencies of the CBF were obtained with a range between 0 and 25 Hz. The first six modes were examined. It can be seen from Figures 5–8 that there was a good agreement between the mode shapes in FEA and EMA. Figure 8 illustrates the motion snapshot of the CBF. Identified frequencies from the FEA and corresponding mode shapes obtained from EMA are summarized in Table 2. It obtained similar results, with differences ranging from 0.55 to 1.87 for the first six modes. There were some differences between the results obtained from the FEA and EMA. The data analysis yielded a correlation coefficient of $R = 0.9875$, a coefficient of determination (r-square) of 0.9752, and a standard error of 1.1148. These statistical measures assess the relationship between a simulated model using FEA as the independent variable and the test results obtained from EMA as the dependent variable in modal analysis.

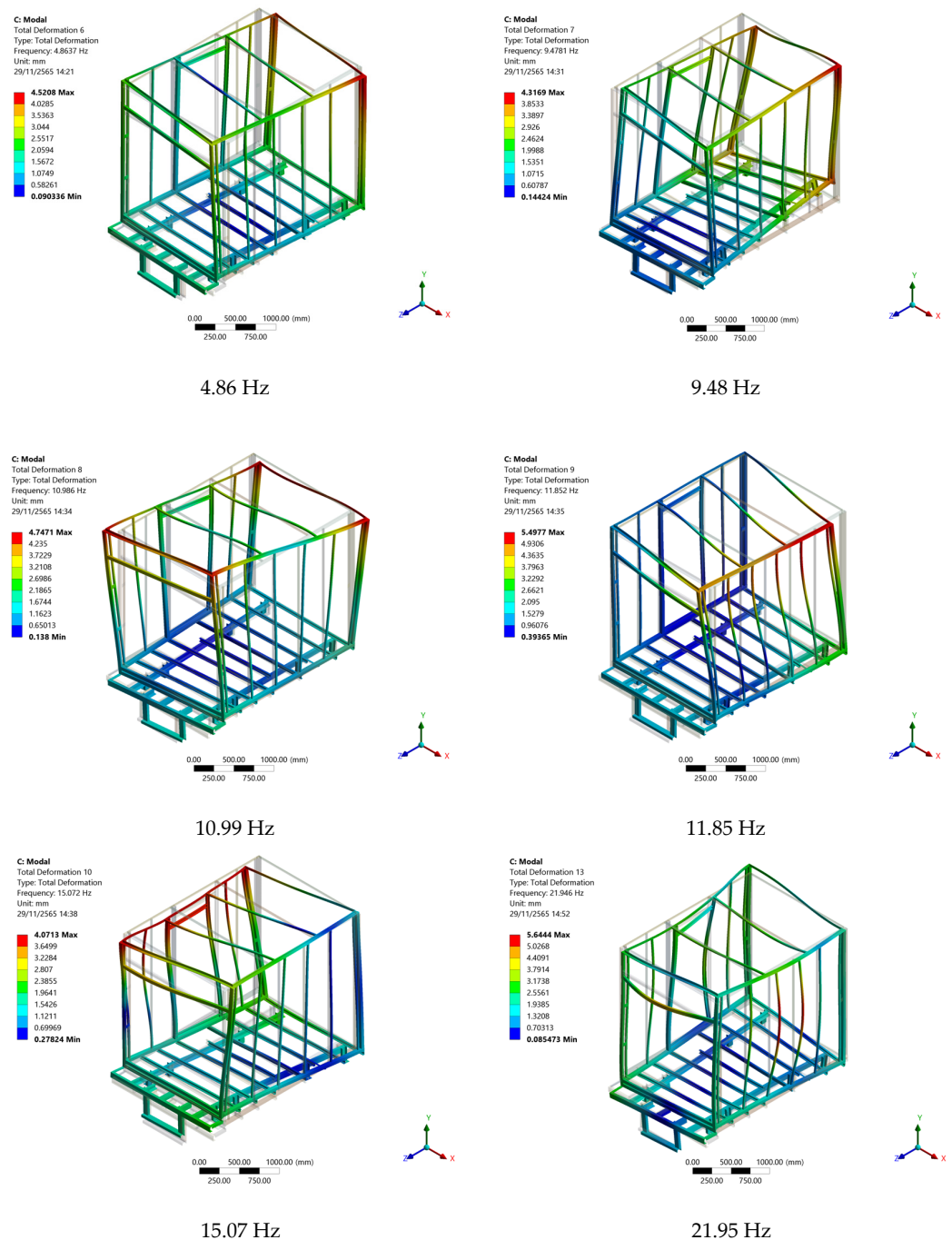


Figure 8. Motion snapshot from relative maximum deviation behavior of FEA.

Table 2. Comparison of natural frequencies found in ANSYS modal and experimental modal.

Freq. Number	FEA (Hz)	EMA (Hz)	Freq. Difference (Hz)
1	4.86	4.31	0.55
2	9.48	8.87	0.61
3	10.99	10.6	0.39
4	11.85	10.9	0.95
5	15.07	13.2	1.87
6	21.95	23.8	1.85

It is thought that these differences resulted from the uncertainties in the structural steel weldment (boundary conditions) of types and material properties of steel. In the FEA, the properties are selected as a density 2.45 g/cm^3 and a Young's modulus of 88.7 GPa , respectively.

In the comparison of natural frequencies in the ANSYS modal and experimental modal, the dominant mode was a lateral bending which occurred in the 4–5 Hz range with maximum translation experienced in alternate between front or rear of the CBF. The second to fifth modes were a torsion in the 8–15 Hz range and a 2-nodal-point lateral bending in the 21–24 Hz range in the sixth mode. Thus, the CBF may experience structural resonance at an idling condition. An increase in mass will reduce the natural frequency, while an increase in the stiffness will increase the natural frequency. Now, the CAD model and material properties can be used to evaluate other analytical models if the mechanical system meets its specifications.

3.2. Refinement and Enhancement

The process of performing a static structural analysis involves the following main steps.

- **Model Preparation:** Create a model of the structure to be analyzed using SolidWorks software. The details are shown in Figures 1 and 2.
- **Meshing:** Divide the model into smaller finite elements through a process known as meshing. Convergence studies were conducted to determine the optimal element size, and it was found that an element size of 10 mm yielded the best results. The finite element model of the CBF utilized a hybrid grid type consisting of 552,400 elements. This modeling approach is similar to the modal analysis simulation.
- **Material Definition:** Specify the material properties for each element in the model. This includes mechanical properties such as the Young's modulus of 88.7 GPa and density of 2.45 g/cm^3 , which define how the material will respond to applied loads.
- **Boundary Conditions:** Apply appropriate boundary conditions to the model, including constraints, loads, and supports. These boundary conditions mimic the real-world environment in which the structure operates. The structure of the CBF is attached to the chassis of a pickup truck with M12 bolts for fastening at eight points, as shown in Figure 9. The structure is designed to carry a total mass of 2000 kg and is uniformly distributed throughout the structure of the refrigerated container floor, calculated from the maximum number of ice loads of 100 bags, with each bag massing 20 kg. The main structure for carrying the load is the upper beam, which is made of seven square tubes, stacked on the C-channel beams. The square tubes of the structure that carries the weight has a size of $3 \times 1\frac{1}{5}$ inches.
- **Analysis Solution:** Run the analysis using the ANSYS solver, which solves the governing equations of static equilibrium to determine the response of the structure under the applied loads. The solver calculates the Total deformation, Equivalent Von-Mises stress, Equivalent Von-Mises strain, Factor of Safety (FOS), and other relevant results for the structure.
- **Analyze and interpret the results** obtained from the analysis. If necessary, refine the model, mesh, or analysis settings based on the results obtained. This iterative process allows for fine-tuning the analysis to achieve more accurate and reliable results. The simulation results suggest that the central part of the structure is the most vulnerable to damage when exposed to a load, with a maximum deformation of 0.41 mm. The

structure experienced a maximum stress of 85 MPa at the connection point between the C-channel beam of the structure and the chassis. However, this area had an FOS value of 2.95. The location with the highest strain of the structure was at the same point as the location with the maximum deformation, with a size of 4.59×10^{-4} mm/mm.

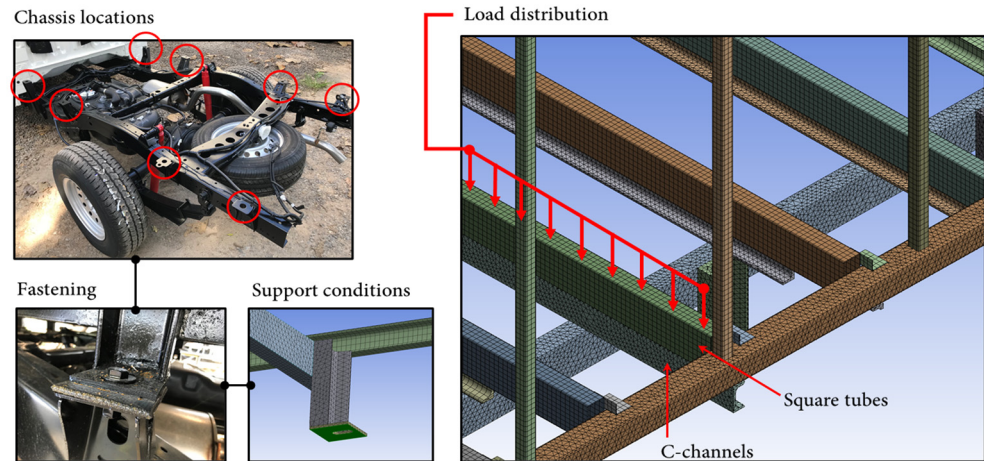


Figure 9. Simulation conditions and loads.

To improve the handling performance of the vehicle, a model of the vehicle's structure was created, and the impact of the mass of the side-swing doors on the structure of the vehicle was considered. The force generated by the mass of the side-swing doors, which is about 30 kg, combined with the total mass of the structure, is equal to 325 kg. After considering the weight exerted on all eight legs of the structure, it was observed that the weight on each leg was not equal. When viewed from above and facing the same direction as the vehicle, the shape of the mass distribution on the legs was tilted towards the left-bottom side of the vehicle, where the side-swing doors are installed. Leg 6 weighed 81 kg, which was more than leg 3 on the opposite side that weighed 49 kg. To improve the position of the CG of the structure, it was necessary to move the center of gravity towards the front as much as possible, by shifting the side-swing doors to the front of the vehicle.

As a guideline for improving the position of the CG of the structure, it is advisable to shift the side-swing door installation towards the front of the vehicle and evaluate the subsequent variation in the center of mass, as shown in Figure 10. Move it three levels from the original position which are 5, 10, and 20 cm, respectively. According to the simulation, the position of the CG of the structure and the forces generated on each leg changed, as shown in Table 3. This causes the mass that each leg bears to shift more towards the front-left direction, which is the direction that improves the balance of the structure. The side-swing door installation position was changed by moving it to the front of the car. It was found that the mass at the position where the leg supports the force decreased at positions G and H by approximately 30%, causing the position of the CG of the structure to change, as shown in Figure 11. The displacement of the center of mass of the structure is directly proportional to the extent to which the side-swing door is moved. Based on the simulation results, it can be concluded that moving the side-swing door installation position 20 cm to the front shifts the position of the center of mass of the structure forward by a distance of 32 cm.

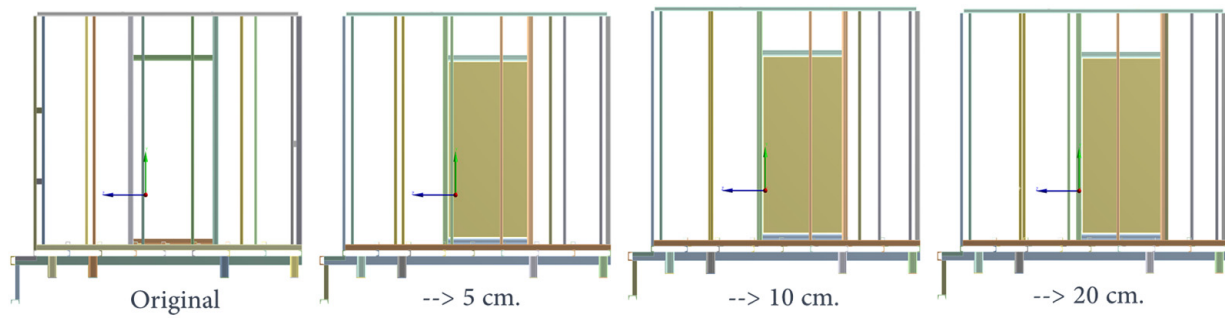
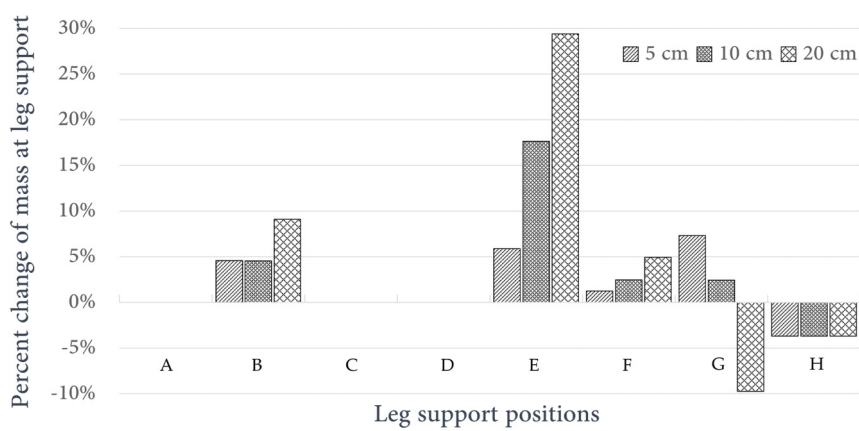


Figure 10. The positions of the side-swing doors’ sliding installation design.

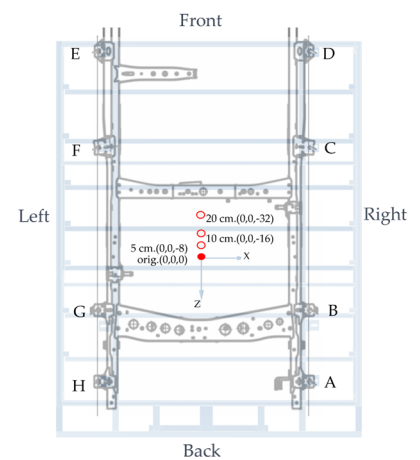
Table 3. The weight at the leg of the CBF structure affecting the chassis (kg).

Leg Support Position	Distance of the Forward Shift in the Installation of the Side-Swing Doors Form Original			
	Original	Shift 5 cm.	Shift 10 cm.	Shift 20 cm.
A	55	55	55	55
B	22	23	23	24
C	32	32	32	32
D	18	18	18	18
E	17	18	20	22
F	81	82	83	85
G	41	44	42	37
H	54	52	52	52

Positions A to H refer to Figure 11b.



(a)



(b)

Figure 11. Changes in (a) percent mass at leg support, and (b) CG position at different distances.

Due to the results of the simulation of the prototype structure in the previous topic, it was found that the structure still had a very high FOS. It is necessary to reduce the size of some parts of the structure to reduce the weight of the structure and save production costs. Therefore, it was decided to reduce the size of the additional structural steel by changing the size of the square tube (ST) to a C-light lip channel (CL) and using an angle steel bar to fasten it to the structure, as shown in Figure 12. Adjusting the size caused it to lesser affect the load behavior compared to the original model, as shown in Table 3.

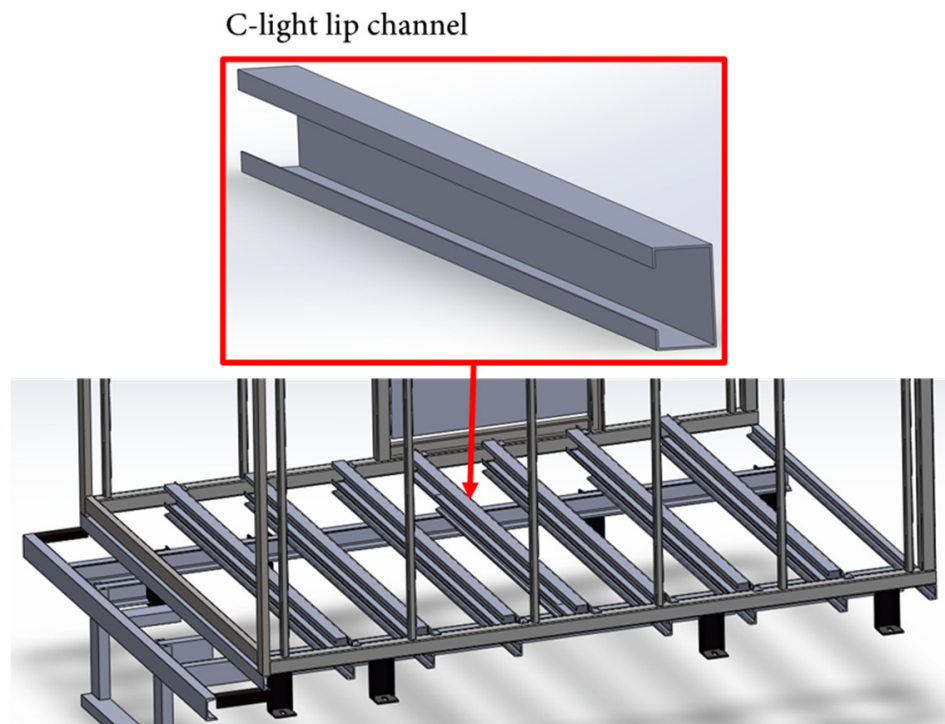


Figure 12. Characteristics of structural improvement.

The structure received a load, along with the side-swing doors that were adjusted by moving the installation position forward by 20 cm, and we found that the structure had collapsed from the load over a distance of 3.1 mm, as shown in Figure 13. In addition, it was found that the maximum stress and strain values were 363 MPa and 1.05×10^{-3} mm/mm, respectively. The position where the maximum strain and stress occurred was on the steel beam used to attach the C-light lip channel beam structure to the main structure, as shown in Figure 14. The aforementioned strain value is in a range that causes the steel to undergo permanent deformation, which poses a significant risk to the structure. In order to prevent damage to the angle steel bar (flat steel) when clamping the top steel beam to the main structure, the thickness of the flat steel used for clamping the beam was simulated to be 1/8 inch or 3.0 mm. The results of the simulation show the maximum force behavior that occurs on the structure, which is presented in Table 4.

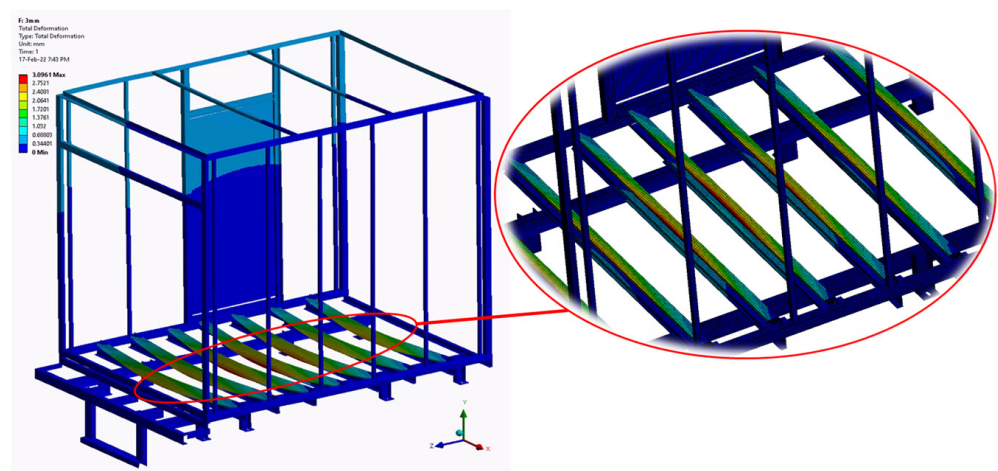


Figure 13. The maximum deformation of the C-light lip channel structural frame.

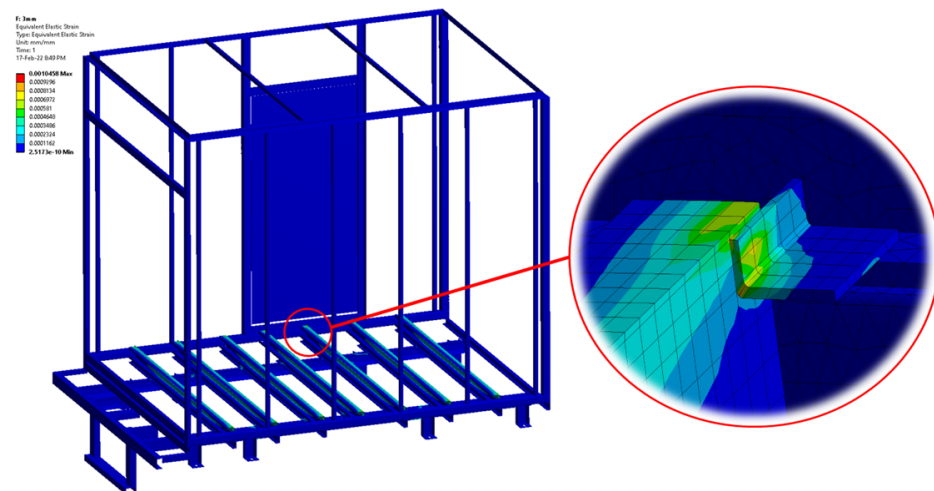


Figure 14. The position of maximum stress and strain.

Table 4. Comparing simulation results of reducing the size of the box beam.

Model	Load	Type	AB's Thickness	Section Sizes	Total Def. (mm)	Stress (MPa)	Strain (mm/mm)	FOS
			inch (mm)	inch (mm)				
01	IB	ST	1/16 (1.5)	3 × 13/16 (76.20 × 30.16)	0.41	85	4.59 × 10 ⁻⁴	2.95
02	IB + SD	ST	1/16 (1.5)	3 × 13/16 (76.20 × 30.16)	0.49	92	5.01 × 10 ⁻⁴	2.71
03	IB + SD	CL	1/16 (1.5)	2 ³ / ₄ × 1 ³ / ₄ (69.85 × 44.45)	3.16	363	2.02 × 10 ⁻³	0.69
04	IB + SD	CL	1/8 (3.0)	2 ³ / ₄ × 1 ³ / ₄ (69.85 × 44.45)	3.10	197	1.05 × 10 ⁻³	1.27

Abbreviation: Ice bag (IB), side-swing door (SD), square tube (ST), C-light lip channel (CL), and angle steel bar (AB).

The simulation results indicate that altering the size of the flat steel impacts the structure’s susceptibility to damage, and it was concluded that a flat steel thickness of no less than 3 mm is necessary to prevent damage to the structure. However, increasing the thickness of the flat steel to more than 3.0 mm does not help to make the structure stronger, because the structure will still tear at the joints with the C-light lip channel due to the thinness and increased deformation of the C-light lip channel. During model simulations 01 and 02, the total mass of the CBF main structure and side-swing door was 325 kg. But when the C-light lip channel was modified in model simulations 03 and 04, the total mass decreased to 319 kg, a reduction of 1.8%. Although this modification caused the FOS value to decrease by approximately 53% from the previous value, the FOS value remained within the acceptable range of the safety standards. In most cases, structural designs include a higher factor of safety, with the exception of the aerospace and automobile industries, where minimizing weight is critical to performance and cost. To achieve this, safety factors are deliberately kept low, typically around 1.25 to 2.0, for the design of structures that must withstand static loads with high confidence, and all available design data are used to ensure their integrity.

3.3. Secure Running Safety Comparison

The load acting on the structure during the installation of the side-swing doors of the refrigerated truck container is significant. A side-swing door was installed on the left side of the CBF structure for the ease of transporting ice bags out of the refrigerated container. The installation of the side-swing door leads to an imbalance in the total weight of the truck. Once the modified truck structure was complete, it was weighed to check the weight

distribution on each side of the wheels. The weight indicator in the rack version of the Dini Argeo, complete with a connector for linking the platforms, is shown in Figure 15. It was found that the weight on each side of the wheels was not balanced, with the weight falling on the left wheel being greater than the right. The details of the topic, Securing Basic Performance and Safety Requirements, will be shown last. Factors affecting the left side structure of the vehicle were the position of the fuel tank combined with the weight of the side-swing doors, and the structure that supports the door force causing the center of mass of the structure to be skewed to the left and located at the rear of the vehicle. This feature was not beneficial for the stability and safety of the vehicle while driving. Therefore, it was necessary to analyze the center of mass of the structure and adjust the appropriate installation position of the side-swing doors.



Figure 15. Front wheel weight (left), rear wheel weight (middle), and weight indicator (right).

The maximum allowable load was reduced when the mass of the finished vehicle (C.W. + A = T) increased, while keeping the G.V.W. fixed. Table 5 shows the chassis and cab curb mass of the base vehicle (C.W.) and the gross vehicle mass of the finished vehicle (G.V.W.) for the models GUN122R-BTFXYT3 and -BTFLXT3.

Table 5. Comparison of wheel mass with accepted basic performance and safety requirements.

Wheel	Side	Mass (kg)			
		Before		After	
Fr	L	495	dif. 15	515	dif. 35
	R	480		480	
Front axle mass (Fr)		975		995	
Re	L	615	dif. 65	590	dif. 40
	R	550		550	
Rear axle mass (Re)		1165		1140	
Total vehicle mass (Fr + Re = T)		2140		2135	
Ratio criteria		45.56% (accept.)		46.60% (accept.)	
G.V.W. criteria		accept.		accept.	
B		≤710		≤715	

Technical specification of single cab mass (kg) [3], model GUN122R-BTFXYT3 and -BTFLXT3, G.V.W.; Fr (1165), Re (1685) and total G.V.W. (2850).

4. Discussion

The high correlation coefficient (R = 0.9875) signified a robust positive linear relationship between the simulated model derived from FEA and the test results obtained through EMA. Moreover, the r-square value indicated that approximately 97.52% of the variability in the test results can be accounted for by the simulated FEA model. The standard error of 1.1148 represents the average deviation between the observed EMA test results and the predicted values obtained from the simulated FEA model. A lower standard error signifies

a more accurate fit of the model in predicting the EMA test results. These findings demonstrate that the FEA model provides a substantial explanation for the observed variation in the EMA test results. Therefore, in the analysis and validation for assessing the failure behavior, the properties were chosen as a density of 2.45 g/cm^3 and a Young's modulus of 88.7 GPa.

The selection of a CL steel section over a ST section can be attributed to two reasons. Firstly, the CL section offers cost advantages as it requires less material compared to a box-shaped section while still providing structural support. Secondly, the CL section offers flexibility in design and installation, allowing for easier customization and adaptation to different construction requirements. However, it is important to note that the CL steel section's open design reduces the cross-sectional area available for carrying loads, resulting in reduced strength and stiffness. This characteristic makes the CL section more susceptible to bending and deformation compared to the ST section. In contrast, the ST steel section is stronger than the CL steel section due to its geometric properties. The ST section has equal thickness on all sides, enabling a uniform distribution of stress and load-carrying capacity. This uniform stress distribution enhances the box-shaped section's ability to resist bending and deformation more effectively.

The results of the comparison of the mass of a CBF four-wheel vehicle before and after modifying the structure and shifting the CG position of the side-swing door towards the front of the car by 20 cm are presented. According to the manufacturer's standards for the GUN122R-BTFXYT3 and -BTFLXT3 vehicle models, the G.V.W. does not exceed the specified values for the front wheel (1165 kg) and rear wheel (1685 kg), and the total G.V.W. is equal to 2850 kg. From the ratio criteria value, it can be seen that the driving safety is 45.56%, which exceeds the requirement of being greater than or equal to 30%. However, the mass affecting the front wheel before modification differs from that affecting the left rear wheel by 65 kg, while the mass of the left and right front wheels differs only by 15 kg, and the mass of the front and rear wheels differs by 50 kg. This could lead to problems with wheel locking during driving.

Regarding the structure after modifying and shifting the CG position of the side-swing door to the front of the car by 20 cm, the mass affecting the left rear wheel decreased, and the difference between the rear wheels reduced by 40 kg (a decrease of 61.5%). Meanwhile, the difference in mass between the left and right front wheels increased by 20 kg. Additionally, the difference in mass between the front and rear wheels decreased from 190 to 145 kg (a decrease of 31%). Although the total vehicle mass before and after the changes differed by only 5 kg, the ratio criteria for driving safety increased to 46.6% without suspension upgrade, ensuring safe driving performance. The total vehicle mass (T) is 2140 kg, which is less than the total G.V.W. limit of 2850 kg, and the maximum mass of passengers, cargo, and baggage (B value) can reach up to 710 kg. However, if loaded to its full capacity of 2000 kg, combined with the total mass before loading of 2135 kg, the total vehicle mass will exceed the total G.V.W. value designed by the manufacturer, which is only 2850 kg. Therefore, if the total G.V.W. exceeds 2200 kg but is not more than 4000 kg, according to the law, an examination must be conducted to evaluate its impact on the reliability, stability, and safety of operation to ensure compliance with engineering principles. The examination must include plans and calculations, along with details of the inspection in the modified or adjusted parts, conducted by a licensed professional engineer to issue a certification letter.

The structure of the CBF has a maximum strain of $1.05 \times 10^{-3} \text{ mm/mm}$, a maximum tensile strength of 197 MPa, and an FOS value of 1.27. The CG was moved forward by 32 mm. Based on the analysis results, the following recommendations are suggested for improving the CBF, although it will remain safe to use even when loaded to its full capacity of 2000 kg that supports cold room panels:

- Use a CL with a size of $2\frac{3}{4} \times 1\frac{3}{4}$ and a thickness of 1/16 inch.
- Use flat steel with a thickness of at least 3.0 mm or 1/8 inch to make the angle steel bar for attaching the channels.

- Move the side-swing door installation position 20 cm forward from the original position, adjust the spacing, and reduce the lateral channels to a suitable distribution range.
- Control the welding process to ensure completeness at every point of the weld.

5. Conclusions

This paper presents the steps involved in conducting a structural analysis to evaluate the strength of a car box frame (CBF) in a four-wheel vehicle. It also focuses on determining the optimal installation location for side-swing doors and cold room panels. To ensure vehicle stability and safety during cargo transportation, the analysis takes into consideration the optimum center of gravity (CG) position. Non-destructive modal methods and finite element analysis were employed to analyze CBF four-wheeled vehicles across various dimensions. The MEscape software was utilized to test the characteristics of the main structure, providing a description of the required equipment for conducting impact operations. This equipment included a conditional motion three-axis accelerometer and a data acquisition module. The analysis process involved several steps, including data collection, processing, mode identification, and result interpretation. By simulating vibrational behavior at different frequencies, a comparison was made using the finite element method in Ansys software to conduct damage analysis under various conditions. Furthermore, the combination of real test results and simulations in both techniques enhanced the accuracy of the analysis and verification process. This paper contributes to the design and manufacture of large CBFs with a significant number of welds, ultimately leading to modified CBF designs that reduce the production costs for the competitive CBF assembly industry.

Author Contributions: Conceptualization, J.S. and N.N.; methodology, N.N.; software, N.N.; validation, N.N., J.S. and K.C.; formal analysis, N.N.; investigation, N.N.; resources, K.C.; data curation, J.S.; writing—original draft preparation, N.N.; writing—review and editing, J.S.; visualization, N.N.; supervision, K.C.; project administration, J.S.; funding acquisition, J.S. All authors have read and agreed to the published version of the manuscript.

Funding: This research was funded by the Suranaree University of Technology (SUT), grant IRD7-707-65-12-03.

Institutional Review Board Statement: Not applicable.

Informed Consent Statement: Not applicable.

Data Availability Statement: Not applicable.

Acknowledgments: The authors are indebted to the Suranaree University of Technology (SUT) and the KRAO Karnchang Limited Partnership, for their generous support and their valuable comments.

Conflicts of Interest: The authors declare no conflict of interest.

References

1. Land Transport Act, B.E. 2522. Available online: http://www.law.moi.go.th/group7_law7.html (accessed on 22 September 2021). (In Thai)
2. Planning Division. *Reports on the Analysis of Freight Transport Operations by Truck*; Department of Land Transport: Bangkok, Thailand, 2022; pp. 1–61. (In Thai)
3. Body Builder's Guide; HILUX 2020. Available online: <https://www.toyota-tech.eu/BBG/BBGN1006/index.pdf> (accessed on 1 January 2021).
4. Matvienko, Y. Safety factors in structural integrity assessment of components with defects. *Int. J. Struct. Integr.* **2013**, *4*, 457–476. [[CrossRef](#)]
5. Singh, A.; Soni, V.; Singh, A.P. Structural Analysis of Ladder Chassis for Higher Strength. *Int. J. Emerg. Technol. Adv. Eng.* **2014**, *4*, 253–259.
6. Poutanen, T.; Lämsivaara, T.; Pursiainen, S.; Mäkinen, J.; Asp, O. Calculation of Safety Factors of the Eurocodes. *Appl. Sci.* **2021**, *11*, 208. [[CrossRef](#)]
7. Gulvanessian, H.; Calgaro, J.-A.; Holicky, M. *Designer's Guide to EN 1990, EUROCODE: Basis of Structural Design*; Thomas Telford Publishing: London, UK, 2002.
8. Longoni, F.; Häggglund, A.; Ripamonti, F.; Pennacchi, P.L.M. Powertrain Modal Analysis for Defining the Requirements for a Vehicle Drivability Study. *Machines* **2022**, *10*, 1120. [[CrossRef](#)]

9. Dawood, S.D.S.; Harithuddin, A.S.M.; Harmin, M.Y. Modal Analysis of Conceptual Microsatellite Design Employing Perforated Structural Components for Mass Reduction. *Aerospace* **2022**, *9*, 23. [[CrossRef](#)]
10. Frankovský, P.; Delyová, I.; Sivák, P.; Bocko, J.; Živčák, J.; Kicko, M. Modal Analysis Using Digital Image Correlation Technique. *Materials* **2022**, *15*, 5658. [[CrossRef](#)]
11. Kong, Y.S.; Abdullah, S.; Schramm, D.; Omar, M.Z.; Haris, S.M. Vibration Fatigue Analysis of Carbon Steel Coil Spring under Various Road Excitations. *Metals* **2018**, *8*, 617. [[CrossRef](#)]
12. Roig, R.; Sánchez-Botello, X.; Escaler, X. Assessment of Novel Modal Testing Methods for Structures Rotating in Water. *Appl. Sci.* **2023**, *13*, 2895. [[CrossRef](#)]
13. Amer, M.; Wallaschek, J.; Seume, J.R. Operational Modal Analysis of an Axial Compressor Rotor and Casing System for the Online Identification of a Digital Twin. *Appl. Mech.* **2022**, *3*, 244–258. [[CrossRef](#)]
14. Garafolo, N.G.; Farhad, S.; Koricherla, M.V.; Wen, S.; Esmaeli, R. Modal Analysis of a Lithium-Ion Battery for Electric Vehicles. *Energies* **2022**, *15*, 4841. [[CrossRef](#)]
15. Falcetelli, F.; Martini, A.; Di Sante, R.; Troncossi, M. Strain Modal Testing with Fiber Bragg Gratings for Automotive Applications. *Sensors* **2022**, *22*, 946. [[CrossRef](#)]
16. Lopes, R.; Farahani, B.V.; Queirós de Melo, F.; Moreira, P.M.G.P. A Dynamic Response Analysis of Vehicle Suspension System. *Appl. Sci.* **2023**, *13*, 2127. [[CrossRef](#)]
17. Fang, J.; Li, X.; Zhang, D.; Zhang, X.; Shao, W. Research on Load Reverse Engineering and Vibration Fatigue Analysis Technology of Rapid Box Wagon. *Materials* **2022**, *15*, 8322. [[CrossRef](#)] [[PubMed](#)]
18. Zhou, X.; Xie, S.; He, M.; Fu, T.; Yu, Q. Research on Vibration Characteristics of 160 km/h Full-Side Open Boxcar Based on Simulation and Test Comparison. *J. Fail. Anal. Prev.* **2023**, *23*, 271–297. [[CrossRef](#)]
19. Hadipour, M.; Alambeigi, F.; Hosseini, R.; Masoudinejad, R. A Study on the Vibrational Effects of Adding an Auxiliary Chassis to a 6-Ton Truck. *J. Am. Sci.* **2011**, *7*, 1219–1226.
20. Barat, V.; Terentyev, D.; Bardakov, V.; Elizarov, S. Analytical Modeling of Acoustic Emission Signals in Thin-Walled Objects. *Appl. Sci.* **2020**, *10*, 279. [[CrossRef](#)]
21. Hou, J.; Wu, Y.; Gong, H.; Ahmad, A.S.; Liu, L. A Novel Intelligent Method for Bearing Fault Diagnosis Based on EEMD Permutation Entropy and GG Clustering. *Appl. Sci.* **2020**, *10*, 386. [[CrossRef](#)]
22. Wang, C.; Huang, H.; Lai, X.; Chen, J. A New Online Operational Modal Analysis Method for Vibration Control for Linear Time-Varying Structure. *Appl. Sci.* **2020**, *10*, 48. [[CrossRef](#)]
23. Ben Ali, J.; Fnaiech, N.; Saidi, L.; Chebel-Morello, B.; Fnaiech, F. Application of empirical mode decomposition and artificial neural network for automatic bearing fault diagnosis based on vibration signals. *Appl. Acoust.* **2015**, *89*, 16–27. [[CrossRef](#)]
24. Feeny, B.; Kappagantu, R. On the physical interpretation of proper orthogonal modes in vibrations. *J. Sound Vib.* **1998**, *211*, 607–616. [[CrossRef](#)]
25. Kerschen, G.; Golinval, J.C.; Vakakis, A.F.; Bergman, L.A. The method of proper orthogonal decomposition for dynamical characterization and order reduction of mechanical systems: An overview. *Nonlinear Dyn.* **2005**, *41*, 147–169. [[CrossRef](#)]
26. MEScopeVES, VES-4000 Modal Analysis. Available online: <http://manuals.vibetech.com/10.%20Modal%20Analysis.pdf> (accessed on 15 November 2020).

Disclaimer/Publisher’s Note: The statements, opinions and data contained in all publications are solely those of the individual author(s) and contributor(s) and not of MDPI and/or the editor(s). MDPI and/or the editor(s) disclaim responsibility for any injury to people or property resulting from any ideas, methods, instructions or products referred to in the content.